Geometric Methods for Modeling and Control of Free-Swimming Fin-Actuated Underwater Vehicles

Kristi A. Morgansen, *Senior Member, IEEE,* Benjamin I. Triplett, and Daniel J. Klein

Submitted as: Regular Paper

Abstract— In this paper, techniques from geometric mechanics and geometric nonlinear control theory are applied to modeling and construction of trajectory tracking algorithms for a free-swimming underwater vehicle that locomotes and maneuvers using a two-link actuated "tail" and independently actuated "pectoral fin" bow planes. Restricting consideration of fluid forces to the simple effects of added mass and quasisteady lift and drag, the resulting system model can be expressed in a control-affine structure. With particular choices of oscillatory actuation of the four system joints, maneuvers such as swimming forward, in and out of plane turning, surfacing, and diving can be constructed. Further, the vehicle and model can generate agile maneuvers such as snap turns. Trajectory tracking can then be produced using state error feedback. The methods are demonstrated both in simulation and in experiment using the University of Washington prototype fin-actuated underwater vehicle.

Index Terms— Biorobotics, underwater vehicle control, nonlinear systems, periodic control, locomotion.

I. INTRODUCTION

Underwater locomotion has long been a subject of interest to the biological community [1], [2], [3], and the robotics and engineering communities have been inspired by this research to construct biologically derived mechanisms that mimic the behavior of individual and groups of swimming lifeforms. The motivation for this work comes from the high maneuverability, low drag and low hydrodynamic noise that fish demonstrate over conventional propeller-driven underwater vehicles. In order to realize a transfer of aquatic biological capabilities to engineered systems, a greater understanding is needed of the interaction of submersed shape-actuated vehicles, the surrounding fluid, and effective means of controlling those vehicles. The work presented here is focused on these tasks.

A. Methodology and Contributions

During the past decade, a variety of mechanical fin-actuated devices have been proposed, built, and studied for purposes of agile autonomous operation. A number of challenges are present in achieving the goal of integrated device and control design that demonstrate the desired agility of dynamic motion in fluids. High fidelity models of dynamic fluid-body interactions are not generally amenable to analytical
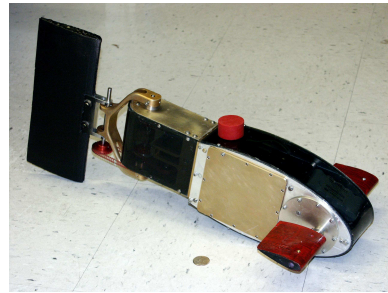
Fig. 1. The UW autonomous fin-actuated underwater vehicle.

control theoretic methods, and kinematics-based models are limited in the types of motion that can be produced as well as in robustness to modeling and design variations. Lower fidelity dynamics models have shown promise for validation of simple system motions, but they have not generally been used for full exploration of system capabilities, particularly for full 3D motion, nor have they been thoroughly validated in hardware implementation. The contributions of this paper, outlined below, were developed with this latter approach in mind: analytical geometric methods for modeling, motion planning and control of shape-actuated mechanical systems operating in a fluid. The specific contributions made here are:

- Expression of the 3D equations of motion of a body with two independently actuated rigid pectoral fins and a tail with arbitrary number of independently actuated rigid links in a form amenable to analysis with tools from geometric control theory;
- Use of geometric control theory to determine open loop controls for motion generation and to determine closed loop feedback stabilization;
- Validation of the model's suitability for capturing agile motions such as snap turns;
- Evaluation of results in both simulation and experiment to validate the methodology.

These results build on prior work of the authors and their colleagues [4], [5], [6], [7], [8]. Except for the results in [6] (a precursor to this paper), the earlier results were restricted to planar systems both in theory and in experiment.

To admit the application of analytical methods, fluid effects are restricted here to a highly simplified quasi-static lift and drag model of the forces on the body and fins. While this quasi-static lift and drag model does not capture every detail of the fluid-body interaction and cannot lead to true performance optimization, it does serve several useful purposes. Primarily,

it allows a description of the system in a control affine form in which the control inputs enter linearly. Existing methods to analyze control performance can then be applied. These methods have been used in prior and related work [4], [5], [7] to consider controllability of the system model and to generate maneuvers that would be difficult to find by intuition and would be unlikely to occur in nature. Further, capturing all fluid flow detail is not always necessary for the purposes of control design, because control feedback can compensate for reasonable modeling errors.

B. Prior Work

The existing results and methodology relevant to the material presented here can be broadly segmented into three categories: modeling, control, and devices. The results discussed here are based on relevance to the topic of analytical modeling and control. A more complete review of existing methods can be found in the tutorial papers by Sfakiotakis [9], Colgate and Lynch [10] and Bandyopadhyay [11].

1) Modeling: Modeling of the fluid dynamics of live fish swimming and of actuated mechanisms in water has received extensive attention. With respect to live fish, Lighthill showed that forward tail-fin locomotion can be represented as a spatial traveling wave along the fish body [2]. Further investigations into forward tail-fin locomotion using fluid dynamics models were made by Churchill [12], Newman and Wu [3] and Wolfgang [13]. Modeling of fast starts and turns have been studied by Weihs [14], [15] and Ahlborn [16], [17] with further live fish studies made by Domenici and Blake [18], Budick and O'Malley [19] and Spiers and van Leeuven [20]. Studies of pectoral fin propulsion and maneuvering in fish have been made by Blake [21], [22], Drucker and Lauder [23], and Gordon et al [24]. With respect to mechanisms, experimental results have been compared to inviscid flow theory and have been used to optimize thrust production [25].

Kinematics models based on biological studies of the shape of a fish body during swimming have been used in a number of instances to generate forward and turning locomotion ([26], [27], [28], [29], [30], [31], [32], [33], [34]) as well as agile maneuvers such as snap turns and fast starts ([35], [36], [13], [37], [38], [29], [39], [40], [41], [42], [43]). In such approaches, the shape of a fish during each step of a maneuver is represented digitally and scaled to the length of the robot of interest. An optimization problem is then solved to find appropriate robot joint angles to match the robot shape as closely as possible to the fish shape at each time step. This approach does produce the desired motions, but requires the optimization problem be re-solved if the number of links or their physical dimensions are altered.

In order to construct dynamics models for fin-actuated underwater vehicles, a number of numerical studies of flow around actuated foils have been pursued to produce appropriate mathematical models of thrust from actuated surfaces [44], [45], [46]. Some of the earliest work with techniques of geometric mechanics and control that applied to fin-actuated systems was produced by Kelly and colleagues [47], [48] where the dynamics of a planar flapping foil with lift of the

form considered here was studied. A geometric mechanics derivation of the equations of motion for a planar three link system without lift or drag was presented in Kanso et al [49] and Melli et al [50]. A key point to note in the unforced system dynamics is that even without lift and drag, the Coriolis terms from the shape dependent mass matrix will cause motion to be produced when the links of the system are actuated. This derivation is closest in style to the approach here, and considered a comparison of the effects of treating added mass of the links independently (an approximation) or coupled accurately (precluding analytical closed form representations). A preliminary version of the dynamics model to be discussed here was presented in the author's work [6]. A number of other planar ([51], [52], [4], [5], [7], [53], [54], [43]) and 3D ([55], [56]) dynamics models have been derived from Euler-Lagrange equations with lift and drag and have been demonstrated for simple forward and turning gaits in simulation.

With respect to vehicles with flexible tails, Kose et al constructed a planar model of flexible tail propulsion using flexible beam theory [57], McIsaac and Ostrowski derived a model of planar anguilliform locomotion without external forcing [58], [59], and Boyer et al have demonstrated 3d locomotion in simulation [60] using a continuum model of the vehicle and elemental quasistatic lift and drag. Dynamics models of pectoral fin actuation were constructed by Chiu et al [61] and validated using data from Kato's experimental work with such devices [62] but without analytical control design.

2) Control: The approaches used to design control for fin-actuated vehicles can be categorized as numerical optimization, adaptive techniques, and geometric methods. As mentioned in the discussion of kinematics models, optimization methods have been used in a number of instances with kinematic models to find robot joint angles to match the robot shape to empirically observed fish behaviors during locomotion [26], [51], [52], [63], [27], [28], [32], [64], [56], [65], [33], [57], [35], [36], [13], [37], [38], [29], [39], [40], [41], [42], [43]. When applied to dynamics models, on the other hand, optimization can be used to find controls that require minimal energy with respect to certain norms (e.g. Saimek and Li [54] and Kanso and Marsden [66]). In order to deal with unmodeled fluid effects and mechanical properties, adaptive techniques such as fuzzy or genetic controllers have been used in the pectoral fin systems of Kato et al [67], [68], [69] and the planar tail-fin vehicles of Kuo and colleagues [43], [34] and Yu et al [29], [30]

Only a few studies have used the approach of geometric nonlinear control theory to produce motion generation or closed loop control of fin-actuated systems. Kelly et al considered the use of geometric nonlinear control methods for motion generation of a planar body in a fluid with forcing from a single point vortex in [47], [48]. McIsaac and Ostrowski constructed gaits for eel-like motion from their planar dynamics models [58], [59] using perturbation methods. In Kanso et al [49], motion generation is demonstrated using a model derived from geometric mechanics, but the motions are not connected to nonlinear control synthesis tools. In Melli et al [50], numerical methods were used to draw connections between the geometric structure of the unforced dynamics and

particular motions in the system. This approach does generate the desired motions but is not a systematic study of the full set of possibilities. To explore the full range of capabilities of the dynamic system with forcing from lift and drag, the authors' early work with planar versions of the system considered here explored the Lie algebraic structure of the forced system dynamics [4], [8], [7]. That work demonstrated connections between the model and capabilities of the system that would likely not be observed in nature, and validated the simplified modeling approach for locomotion in the plane. These results were then addressed with averaging theory to construct feedback control for trajectory tracking [5], [7], [70], [8]

3) Devices: The earliest demonstrated fin-actuated hardware systems came out of MIT and Draper Laboratories with the Robopike, Robotuna and VCUUV projects [71], [28], [26], [27]. Robopike and Robotuna were constrained to planar motion in flow tunnels, but the VCUUV was capable of full 3D motion using actuated bow planes. On the opposite end of the size spectrum, a microscale free swimming 3D robot with both tail fin locomotion and pectoral fin maneuvering has been built by Deng and Avadhanula [72], and preliminary experimental results for fin actuation, but not directional motion generation or tracking, were presented. Experimental results for flapping foils generating thrust were compared to control theoretic models by Yamaguchi and Bose [73], Kelly et al [47], Read et al [74], Saimek and Li [54], Licht et al [31]. Planar vehicles with tail-fin actuation have been demonstrated in [52], [75], [29], [30], [32], [65], [64], [34], and 3D vehicles with tail-fin actuation and pectoral fin depth control have been demonstrated in 3D in limited cases by Kim and Youm [55], Wang et al [56] and Zhou et al [33] (also demonstrated depth control) and Ziegler et al [40]. Extensive work with planar systems propelled using pectoral fins has been performed by Kato and colleagues [67], [68], [69] demonstrating the ability to both propel forward, turn and follow desired trajectories. Snap turns and fast starts have been demonstrated in [35], [36], [13], [37], [38], [29], [39], [40], [41], [42], [43]. Experimental work by the authors of this paper includes planar vehicles [4], [5], [7] and early work with fully 3D vehicles in [6].

Devices with actuated flexible fins are also in development for a number of applications. At a large scale is the device built by Davies et al [76] in emulation of a ribbon fin. An eel-like robot with five links was built by McIsaac and Ostrowski [59] and used to demonstrate their theoretical methods [58] and flexible fins for hovering have been demonstrated in [77]. At a smaller scale, tailfin actuated microbots with buoyancy control of depth has been built by Guo et al [53] and Kosa et al [57].

C. Organization of the Paper

The paper is organized as follows. In Section II, the design and physical properties of the experimental fin-actuated robot shown in Fig. 1 are presented. A system model amenable to geometric control theoretic methods is then presented in Section III. An important aspect of this model is that its applicability is not limited to the specific system here with a two-link tail, but is general enough to encompass a tail with an arbitrary number of discrete links. Motion generation and control inputs to generate particular gaits are given in Section IV. The controls are demonstrated in simulation and in experiment in Section V. A comparison of these results shows that the extremely simple model does in fact capture the qualitative behavior of the physical system, and feedback control produces the desired trajectory tracking capabilities. Further, this model can be used to produce agile maneuvers such as snap turns. Concluding remarks and directions of ongoing work are given in Section VI.

II. EXPERIMENTAL SYSTEM

The physical device being used in the work discussed here is shown in Fig. 1. The body of the robot has two sealed compartments composed of aluminum side or top panels wrapped with heat-molded semi-transparent acrylic. The forward body compartment contains the microcontroller board, Phytec MPC555 with Freescale MPC555 PowerPC microprocessor, mated to a custom made motherboard, sensing and communication devices, pectoral fin servo motors, and batteries. The aft compartment contains the servo motors for the two tail links. The tail itself is composed of a wishbone shaped "peduncle" region and a rectangular-planform thin hydrofoil (NACA 0012) with chord length 8cm and span 25.4 cm for the "caudal" fin. The tail joints are actuated with Hitec HS-5945MG high-torque (peduncle) and HS-5925MG high speed (caudal) servo motors, respectively capable of 0.847 Nm and 1.27 Nm torque at 6V. The two "pectoral" fins located at the front of the body are independently actuated by Hitec HS-5925MG high-speed servos.

The onboard sensors consist of a 3D compass, Honeywell HMR3300, which can measure 360 degrees of yaw and ± 60 degrees of roll and pitch, and a pressure sensor, Druck PDCR4010, able to measure depth with a resolution of 0.016atm. Data collection, processing, and control function generation are handled onboard by the microcontroller. The microcontroller has roughly 4 MB of memory which allows for the collection of trajectory data (orientations, depth, time, servo commands, and received data). When operated in the indoor test tank, the robot is equipped with a 72MHz RC receiver, model Electron 6 from Hitec. The robot is capable of decoding data on this frequency for either remote control or autonomous operation. In the remote control mode, the received data consists of low-level commands, such as tail joint frequency and depth set point. In the autonomous mode, the received data consists of spatial position information which is transmitted by an external tracking system (discussed later in this section).

Physical dimensions of the robot are shown in Fig. 2. The overall weight is approximately 3kg. The centers of buoyancy and gravity are engineered to be co-linear (but not coincident) along the body x_3 axis. The pectoral fins are composed of dense styrofoam covered with fiberglass and are located forward and above the center of mass. The fins have the NACA 0012 hydrofoil profile with chord length 11.3cm and span 7.8cm. The lift force generated by each fin is assumed to act at its quarter chord point.
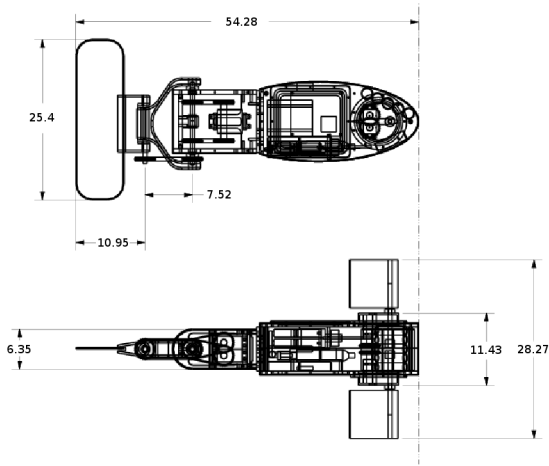
Fig. 2.   Physical dimensions of the robot (in cm).

Fig. 3.   Free body diagram of robot showing modeled lift and drag forces.

Given the limited onboard sensor suite and the nonlinear dynamics of the vehicle, onboard full state estimation is extremely challenging. Therefore, an external real-time vision system consisting of four identical underwater cameras connected to a central computer was designed and implemented. Each camera, model CVC320WP from CSI Speeco, is connected to its own Osprey 100 capture card in the central computer, which is an Intel Pentium 4 2.4GHz machine running Linux. Grayscale video frames of resolution 320×240 are simultaneously captured from each camera at rates up to 30Hz. To maximize the available workspace, the cameras are mounted in the upper corners of the test tank, at a depth of approximately 18cm. Observation data collected online consists of blob centroid features extracted from each image. These features are obtained by first subtracting the static background and then running a blob detector on the thresholded difference between the current image and the background.

A particle filter [78] is run on the central computer, and the resulting state estimate is transmitted via radio communication to the robot. Propagation is achieved using a Frenet-Serret model with variable speed and a zero order hold on control inputs. This model is a decent first-order approximation of the robot body motion and more importantly, can be processed quickly in order to meet the real-time constraint. Because the estimator does not know which control inputs the robot is applying, zero-mean Gaussian noise is assumed for each input. The observation model of the particle filter relies upon a Tsai camera calibration [79], [80] generated from known world to image point correspondences. This calibration allows each particle to be projected into each image. The probability of the observation given the projected particle state is Gaussian based on image distance, and each camera is assumed to be independent. Resampling is done after each update, and a total of 1500 particles are used.

III. MODELING

One of the primary foci of this work is to explore the connection between bio-inspired underwater vehicles and analytic nonlinear dynamics and control theory. Therefore the system model needs to be based on analytical representations
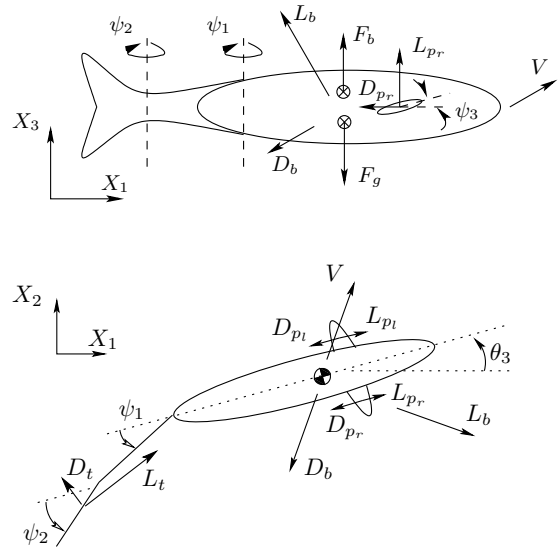
rather than numerical calculations or empirical data. Clearly this choice will place limits on the accuracy of the modeled behavior relative to the true system performance, however, in the context of autonomous vehicle operation, small differences can be mitigated with feedback control. The validity of this approach is considered in the following sections, as well as in related works [4], [5], [7], via the comparison of simulation and experimental results.

The fluid in which the robot is operating is assumed to be inviscid, irrotational and incompressible as well as infinite in domain, and three-dimensional fluid effects will be neglected. Any rigid body moving in a fluid environment will cause movement of the surrounding fluid which can be modeled with an appropriate set of fluid state variables. For simplicity however, the state of the fluid will not be explicitly monitored here, but rather its interaction with the robot mechanism will be treated as externally applied lumped forces. When a rigid body accelerates in a fluid, a portion of the surrounding fluid also accelerates. As the state of the fluid is not being modeled, this change in fluid energy is accounted for by assuming an apparent increase in the mass of the object, termed added mass, in the direction the object is accelerated. Additionally, as fluid elements move relative to one another and around solid bodies, pressure differentials develop. When summed up, these incremental differentials result in net forces typically resolved into orthonormal components termed lift and drag. Viscosity in a fluid will also produce drag on a body often referred to as skin friction, but the fluid here is assumed inviscid and this type of drag is therefore neglected. Given the composition of the system here (body, two-link tail, and two pectoral fins), the set of external forces on the system is then lift and drag from the tail, L_t and D_t, lift and drag from the body, L_b and D_b, lift and drag from the two pectoral fins, L_{p_r}, L_{p_l}, D_{p_r}, and D_{p_l}, the force of buoyancy, F_b, the force of gravity, F_g, and the moments resulting from these forces. A free body diagram of the system with these forces is shown in Fig. 3.

A. Unforced equations of motion for the body segment

The position and orientation of the body segment of the robot are denoted by $g \in SE(3)$ which can be written in homogeneous matrix notation as

$$g = \begin{bmatrix} R & x \\ 0 & 1 \end{bmatrix}, \tag{1}$$

where $R \in SO(3)$ is the orientation of the body, and $x \in \mathbb{R}^3$ is the position of the center of mass of the body, both relative to a fixed inertial reference frame. Here the longitudinal axis of the body is taken to be the x_1 axis (positive forward), the lateral axis to be the x_2 axis (positive to the left), and the x_3 axis to be positive upward. ZYX Euler angles are used to determine the rotation matrix from the body orientation vector θ in the analysis and simulations below. The body-fixed translational and angular velocities are denoted by the vectors V and Ω. In this notation, the velocity of the body is given by

$$\dot{R} = R\widehat{\Omega} \tag{2}$$
$$\dot{x} = RV \tag{3}$$

where $\widehat{\Omega} = \begin{bmatrix} 0 & -\omega_3 & \omega_2 \\ \omega_3 & 0 & -\omega_1 \\ -\omega_2 & \omega_1 & 0 \end{bmatrix}$ contains the angular

rotation rates $\omega_i = \dot{\theta}_i$.

For an incompressible, irrotational and inviscid fluid, the unforced equations of motion of a single *rigid* body may be written using Kirchoff's equations [81]:

$$J\dot{\Omega} = J\Omega \times \Omega + MV \times V \tag{4}$$
$$M\dot{V} = MV \times \Omega \tag{5}$$

where J and M are the inertia and mass matrices including added mass effects. Defining the momentum of the robot body (without the tail) as $\tilde{p} = [\Pi, P] = [J\Omega, MV]$, these equations can be expressed as

$$\dot{\tilde{p}} = \begin{bmatrix} \Pi \times \Omega + P \times V \\ P \times \Omega \end{bmatrix}. \tag{6}$$

Approximating the body segment as an ellipsoid of mass m with body axes given by a_{x_1}, a_{x_2} and a_{x_3}, the added mass in all three axes is $\frac{4}{3}\pi\rho a_{x_1} a_{x_2} a_{x_3}$ [82]. The moment of inertia about x_1 is $J_1 = \frac{1}{5}m(a_{x_2}^2 + a_{x_3}^2)$ with added inertia term $\frac{4}{15}\pi\rho a_{x_1} a_{x_2} a_{x_3}(a_{x_2}^2 + a_{x_3}^2)$ and similarly for the other two axes. The two tail links will be modeled as flat plates with no added mass in the x_1 or x_3 directions and no added inertia about x_2. Added mass for the x_2 direction of a flat plate is $\frac{1}{4}\rho\pi l^2 h$ (l and h are respectively the length and height of the plate), and the added inertias are $2\pi\rho(\frac{l}{4})^4 h$. For simplicity of calculation, the components of the mechanism will be assumed to be hydrodynamically decoupled (i.e. added masses are independent). For a comparison of results with this assumption to results with coupled added mass calculations, the reader is referred to [49]. For simplicity, the pectoral fins are assumed to have no added mass.

B. Potential forces

The vehicle is assumed to be neutrally buoyant with centers of buoyancy and gravity that are non-coincident but are co-located along an axis parallel to the body x_3 axis. The direction of gravity, in the body-fixed coordinate frame, is given by $\Gamma = R^T k$ where $k = [0, \ 0, \ -1]^T$. If the vector from the center of mass to the center of buoyancy is $r_b = [0, \ 0, \ h_b]^T$, then the effect of the non-coincident forces is a net torque $-\frac{1}{2}m\gamma\Gamma \times r_b$ where γ is the magnitude of the gravitational force.

C. Forces on heaving and pitching hydrofoils

Each of the pectoral fins can pitch, and the tail fin can pitch and heave, with arbitrary frequency. Using results from [45] to determine the lift forces under the assumption that all shed vortices are neglected gives

$$L_{f1} = 4\pi d V_{f1}(V_{f1} + d\omega_f), \quad L_{f2} = 4\pi d V_{f2}(V_{f1} + d\omega_f), \tag{7}$$

where L_{f1} is the force generated along the chord of the foil, and L_{f2} is the force generated out of the chord/span plane. The quarter chord location of the foil is denoted by d, while V_{f1} and V_{f2} are the speeds of the foil in its body-fixed x_1 and x_2 directions, respectively. The angular rate of the foil about its leading edge is denoted ω_f.

Notice that in this formulation, the angle of attack of the foil does not explicitly appear in the equations as the fluid is assumed to be at rest, so the angle of attack is implicit in the definition of the forces. Furthermore, as three dimensional fluid effects are not being considered here, the aspect ratio and the effect of the body next to the pectoral fins have been neglected.

D. Lift and drag on the body

To allow use of planar results, the lift and drag will be calculated in each plane, and the lift and drag will be assumed negligible in the x_2-x_3 plane. Because the body is an ellipsoid rather than a thin pitching and heaving plate, lift and drag on the body of the robot are assumed to be generated in the usual steady fashion. Under these assumptions, the lift on the body is

$$L_{b,12} = \frac{1}{2}\rho c_{lb,12}\alpha_{12}A_{b,12}\left(V_1^2 + V_2^2\right), \tag{8}$$
$$L_{b,13} = \frac{1}{2}\rho c_{lb,13}\alpha_{13}A_{b,13}\left(V_1^2 + V_3^2\right), \tag{9}$$
$$\tag{10}$$

where $c_{lb,12}$ and $c_{lb,13}$ are the lift coefficients per angle of attack α_{12} in the $x_1 - x_2$ plane, and α_{13} in the $x_1 - x_3$ plane. The planform area of the body is given by $A_{b,12}$ in the x_1-x_2 and $A_{b,13}$ in the $x_1 - x_3$ plane. As in Fig. 3, the velocity of the body is V, and ρ is the density of the fluid. The drag is computed in a similarly to the lift as

$$D_{b,12} = \frac{1}{2}\rho(c_{db0} + c_{db,12}\alpha_{12}^2)A_{b,12}\left(V_1^2 + V_2^2\right), \tag{11}$$
$$D_{b,13} = \frac{1}{2}\rho(c_{db0} + c_{db,13}\alpha_{13}^2)A_{b,13}\left(V_1^2 + V_2^2\right), \tag{12}$$

where c_{db0} is the zero lift drag coefficient of the body, $c_{db,12}$ and $c_{db,13}$ are the drag coefficients per square angle of attack for the $x_1 - x_2$ and $x_1 - x_3$ motions of the body respectively.

Lastly, the fluid is known to add a damping effect to rotations of the body about its principal axes, as the rotating body will induce separated flow about its bluff edges which will transfer rotational kinetic energy from the body to the fluid. This effect is somewhat crudely, but effectively, included in the model as a simple viscous moment that impedes body rotation in all directions,

$$M_{damp} = -c_m \Omega, \tag{13}$$

where c_m is a simple damping coefficient.

E. Forced equations of motion

For systems such as this one where forces on the system are independent of the body position and orientation, Lagrange-Poincaré equations can be used to describe the system dynamics. The relevant information will be stated below, and the reader is referred to the references (e.g. [83], [84]) for full detail. A mechanical system of the type considered here can be described by the states of the main body, g, termed group states, in combination with the values of the states that describe the relative placement of the moving components to the main body, denoted r and termed the shape states. Here the shape states r are the tail joint angles, $r = [\psi_1, \psi_2]^T$. The effect of the pectoral fins is assumed to be limited to generation of lift forces, and they are not included in the system momentum or added mass.

Recall [84] that the Lagrangian for a system of k links with states $r, g, \dot{r},$ and $\dot{g}$ can be written as

$$L(r, g, \dot{r}, \dot{g}) = \frac{1}{2} \sum_{i=1}^{k} V_i^T(r, g, \dot{r}, \dot{g}) M_i(r, g) V_i(r, g, \dot{r}, \dot{g})$$
$$- U(r, g) \tag{14}$$
$$= \frac{1}{2} \begin{bmatrix} \dot{r} \\ \dot{g} \end{bmatrix}^T M(r, g) \begin{bmatrix} \dot{r} \\ \dot{g} \end{bmatrix} - U(r, g), \tag{15}$$

where $U(r, g)$ is potential energy (from buoyancy and gravity), and V_i and M_i correspond to the body-fixed velocity and mass matrix of each of the links in the system. Because the mass matrix for an immersed mechanical system will change based on the joint angles r, but not based on the group states g, the Lagrangian can be rewritten using the body-fixed velocity of the group states, $\xi = g^{-1}\dot{g}$, to give the reduced Lagrangian:

$$l(r, \dot{r}, \xi) = L(r, e, \dot{r}, \xi) \tag{16}$$
$$= \frac{1}{2} \begin{bmatrix} \dot{r} \\ \xi \end{bmatrix}^T M(r) \begin{bmatrix} \dot{r} \\ \xi \end{bmatrix} - U(r, e) \tag{17}$$
$$= \frac{1}{2} \begin{bmatrix} \dot{r} \\ \xi \end{bmatrix}^T \begin{bmatrix} m(r) & \mathcal{A}^T(r)\mathcal{I}(r) \\ \mathcal{I}(r)\mathcal{A}(r) & \mathcal{I}(r) \end{bmatrix} \begin{bmatrix} \dot{r} \\ \xi \end{bmatrix}$$
$$- U(r, e) \tag{18}$$

where the last equation is simply a re-expression of the previous where $e \in SE(3)$ is the identity element, $\mathcal{A}(r)$ is termed the local connection, $\mathcal{I}(r)$ is termed the local form of the locked inertia tensor, $M(r) = M(r, e)$ is termed the

reduced mass matrix, and $m(r)$ is the shape mass matrix. The Lagrange-Poincaré equations are then

$$g^{-1}\dot{g} = \xi = -\mathcal{A}\dot{r} + \mathcal{I}p \tag{19}$$
$$\dot{p} = ad_\xi^* \frac{\partial l}{\partial \xi} + F_\xi \tag{20}$$
$$\mathcal{M}_{rr}(r)\ddot{r} = \frac{\partial l}{\partial r} + F_r. \tag{21}$$

The first equation (19) describes how to obtain the body motion from the momenta and shape, and for the system here is just a re-expression of (3) which states $\dot{R} = R\widehat{\Omega}$ and $\dot{x} = RV$. In the second equation (20), p is the bulk system momentum which includes the effects of the tail motion, and F_ξ are the external forces of lift and drag from all fins and the body. The term $ad_{\xi_1}^* \xi_2$ is the coadjoint or dual to the Lie Bracket (discussed below). Here the operation is simply given by (6) replacing $[\Omega, V]$ with ξ and $[\Pi, P]$ with $\frac{\partial l}{\partial \xi}$. The final equation (21) describes the controlled physical shape of the system, which reduces to $\ddot{r} = F_r$ because the shape here is fully controlled. The term $\mathcal{M}_{rr} = m(r) - \mathcal{A}^T \mathcal{I} \mathcal{A}$ is the kinetic energy matrix for the shape states.

IV. NONLINEAR CONTROL

In order to evaluate the validity of the model in the previous section relative to the actual robot, the first question that must be addressed is how to determine controls that will generate desired motion primitives. The model derived here is known not to be feedback linearizable (see e.g. [4], [5], [7]) due to the particular nonlinear structure of the components, however, pairings of control and motion primitives can be accomplished using geometric nonlinear control methods.

A. Accessibility

To evaluate accessibility, (19)-(20) must be rewritten in the form

$$\dot{z} = f_0(z) + \sum_{i=1}^{m} f_i(z)u_i(z, t) \tag{22}$$

where m is the number of control inputs and here is equal to four for the number of actuated joints. Specifically u_1, u_2, u_3, u_4 are respectively the inputs to the first and second tail joints, the right pectoral fin, and the left pectoral fin. As stated above, the tail fin actuation enters the system as torque inputs to (21) as $F_r = \begin{bmatrix} u_1 \\ u_2 \end{bmatrix}$. The pectoral fin actuation appears in the system equations as velocities in the lift terms which are nonlinear functions. In order to achieve the form (22) in which controls only appear linearly, the system states can be augmented with states $\psi_3, \dot{\psi}_3, \psi_4,$ and $\dot{\psi}_4$:

$$\ddot{\psi}_3 = u_3 \tag{23}$$
$$\ddot{\psi}_4 = u_4. \tag{24}$$

The overall system state is then $z = [g^T, r^T, \psi_3, \psi_4, \dot{g}^T, \dot{r}^T, \dot{\psi}_3, \dot{\psi}_4]^T$ where $z \in SE(3) \times \mathbb{R}^2 \times \mathbb{R}^2 \times se(3) \times \mathbb{R}^2 \times \mathbb{R}^2$.

In (22), $f_0(z)$ is termed the system drift vector field, and $f_i(z)$ are termed the system control vector fields. With the

given definition of the state z, the control vector fields are unit basis vectors: $f_1 = e_{17}, f_2 = e_{18}, f_3 = e_{19}, f_4 = e_{20}$ and correspond, in order, to the first and second tail joints, and the right and left pectoral joints. The vector fields dictate how the system state evolves over time with and without control actuation. Motion forward or backward along individual control vector fields can be created by setting the appropriate controls to constant values with the appropriate signs. To determine the effects of more complicated time-varying controls, the Lie brackets of vector fields can be computed and analyzed.

Recall that the Lie bracket of two vector fields f_i and f_j is another vector field denoted $[f_i, f_j]$ defined by

$$[f_i, f_j] = \frac{\partial f_j}{\partial z} f_i - \frac{\partial f_i}{\partial z} f_j. \quad (25)$$

The Lie bracket also satisfies the properties:

$$\begin{align}
[f_i, f_i] &\equiv 0 \quad &(26)\\
[f_i, f_j] &= -[f_j, f_i] \quad &(27)\\
[f_i, [f_j, f_k]] &= -[f_j, [f_k, f_i]] - [f_k, [f_i, f_j]]. \quad &(28)
\end{align}$$

Lie brackets between control vector fields correspond to particular combinations of oscillatory, or area generating, motions of the associated control input functions. These vector fields then determine what system motion will be accomplished if the corresponding control input functions are applied to the system. An important point to note is that while those control inputs will generate the given motion along the vector field, they may also generate motion in other vector field directions.

1) Forward locomotion and heading control: Determining the motions to which vector fields correspond at all states in a system with this level of complexity is generally quite difficult. However, as the vector fields are analytic, they can be evaluated for representative physical parameters and analyze the result for particular operating conditions. Straightforward, but involved, calculations have then shown in previous work [4] the following correspondence between vector fields and motion directions:

$$\begin{align}
\dot{\psi}_1 &\leftrightarrow f_1 \quad &(29)\\
\dot{\psi}_2 &\leftrightarrow f_2 \quad &(30)\\
\dot{x}_1 &\leftrightarrow [[f_0, f_1], [f_0, f_2]] \quad &(31)\\
\dot{\theta}_3 &\leftrightarrow [f_1, [f_0, [f_1, [f_0, f_2]]]]. \quad &(32)
\end{align}$$

From this correspondence direct motion can be generated in the x_1 and θ_3 directions. Note that the Lie bracket calculations are made before evaluating at particular states, so $f_0 = 0$ does not imply $[f_0, f_i] = 0$. Motion in the x_2 direction is coupled with the θ_3 direction, and an additional spanning vector field has not been found. However, as trajectory tracking in the plane can be accomplished as long as a vehicle can move forward and turn with a finite radius, the robot can move between any two points in the plane with arbitrary initial and final orientation. The lack of the final vector field simply precludes such motions happening on arbitrary time scales. Note that these Lie bracket- direction pairs correspond to the dominant effect produced. If biases are introduced into the controls that will be discussed below, the term θ_3, for example, cold be generated by the Lie Bracket in (31) in addition to $\dot{x}_3$.

2) Forward locomotion and pItch control: To evaluate the additional motions that can be generated by oscillating the pectoral fins, consider only the vector fields that correspond to those two fins. In this case, again evaluating the vector field parameters at representative values used in the simulations below, the following can be found (see e.g. [6]):

$$\begin{align}
\left\{\dot{x}_1, \dot{\theta}_3\right\} &\leftrightarrow [f_3, [f_0, f_3]] \quad &(33)\\
\left\{\dot{x}_1, -\dot{\theta}_3\right\} &\leftrightarrow [f_4, [f_0, f_4]] \quad &(34)\\
\dot{x}_1 &\rightarrow [[f_3, f_0], [f_4, f_0]]. \quad &(35)
\end{align}$$

In the first two Lie bracket vector fields, the use of a single fin will generate both forward propulsion as well as a yaw turn. The turns generated by each of the fins are opposite in direction, so in the third case where both fins are being used, no net turn is generated. As in the previous set of vector fields, additional motions can be generated by introducing a bias into the controls. Here a bias will generate pitch and depth, $\dot{\theta}_1$ and $\dot{x}_3$.

B. Motion Generation

For certain classes of nonlinear systems, including the one to which the system here corresponds, the use of superimposed periodic inputs with particular frequency relations has been shown to generate motion in desired directions that cannot be directly actuated. A particular set of oscillatory signals applied to the actuators of a system which results in a characteristic (stable) system response is generally referred to as a "gait". One method to construct gaits and produce motion in desired directions is to use a knowledge of the system Lie brackets, discussed in the previous section, and an application of averaging theory. Full details of the work below may be found in [70].

To form a correspondence between oscillatory inputs and Lie brackets, each of the control functions u_i is chosen to be of the form

$$u_i(z, t) = u_{i0}(z) + \sum_{j=1}^{m} u_{ij}(t) \sin\left(\frac{2\pi}{T}\omega_{ij}t + \phi_{ij}\right) \quad (36)$$

where $\omega_{ij} \in \mathbb{Z}$, $\phi_{ij} \in \mathbb{S}^1$, and $i \in 1, \ldots, m$. These controls u_i are then the sum of a purely state dependent term and a set of T-periodic functions. The system (22) can be rewritten as

$$\dot{z} = \tilde{f}_0(z) + \sum_{i=1}^{m} \tilde{f}_i(z, t), \quad (37)$$

where

$$\begin{align}
\tilde{f}_0(z) &= f_0(z) + \sum_{i=1}^{m} f_i(z)u_{i0}(z) \quad &(38)\\
\tilde{f}_i(z, t) &= \sum_{ij} f_i(z)u_{ij}(t) \sin\left(\frac{2\pi}{T}\omega_{ij}t + \phi_{ij}\right). \quad &(39)
\end{align}$$

Note that the $\tilde{f}_i$ are T-periodic by construction. Additionally T is assumed to be small, and the functions $u_{ij}(t)$ are assumed

to satisfy

$$\int_0^T (u_{ij}(s_1) - u_{i0})ds_1 = 0 \tag{40}$$

$$\int_0^T \int_0^{s_2} (u_{ij}(s_1) - u_{i0})ds_1 ds_2 = 0. \tag{41}$$

The following results can then be proved.

Lemma 4.1 ([70]): Motion in the direction $[f_i, [f_0, f_j]]$ can be generated with control functions of the form

$$u_i(z,t) = u_{i0}(z) + u_{i1}(t)\sin\left(\frac{2\pi}{T}\omega t\right) \tag{42}$$

$$u_j(z,t) = u_{j0}(z) + u_{j1}\sin\left(\frac{2\pi}{T}\omega t\right) \tag{43}$$

or of the form

$$u_i(z,t) = u_{i0}(z) + u_{i1}(t)\cos\left(\frac{2\pi}{T}\omega t\right) \tag{44}$$

$$u_j(z,t) = u_{j0}(z) + u_{j1}\cos\left(\frac{2\pi}{T}\omega t\right). \tag{45}$$

where u_{j1} is a constant. If $i = j$, the definition for u_i is used.

Note that if $i = j$ above, only positive motions along the vector field will be possible, meaning that the gait cannot be reversed.

Lemma 4.2 ([70]): Motion in the direction $[[f_0, f_i], [f_0, f_j]]$ can be generated with control functions of the form

$$u_i(z,t) = u_{i0}(z) + u_{i1}(t)\cos\left(\frac{2\pi}{T}\omega t\right) \tag{46}$$

$$u_j(z,t) = u_{j0}(z) + u_{j1}\sin\left(\frac{2\pi}{T}\omega t\right). \tag{47}$$

where u_{j1} is a constant.

Lemma 4.3 ([70]): For motions in the direction $[f_i, [f_0, [f_j, [f_0, f_k]]]]$, define the following:

$$\chi(\alpha) = \cos\left(\frac{2\pi}{T}\alpha\omega t\right). \tag{48}$$

Motion in this direction can then be generated with control functions determined by the following three cases:

(a) $i = j = k$:

$$u_i(z,t) = u_{i0}(z) + u_{i1}(t)\chi(1); \tag{49}$$

(b) $i = j$ or $i = k$ or $j = k$: Assume $i = j$ and make similar choices in the other two cases:

$$u_i(z,t) = u_{i0}(z) + u_{i1}\chi(1) \tag{50}$$
$$u_k(z,t) = u_{k0}(z) + u_{k1}(t)\chi(2) \tag{51}$$

where u_{i1} is a constant;

(c) $i \neq j \neq k$:

$$u_i(z,t) = u_{i0}(z) + u_{i1}(t)\chi(3) \tag{52}$$
$$u_j(z,t) = u_{j0}(z) + u_{j1}\chi(2) \tag{53}$$
$$u_k(z,t) = u_{k0}(z) + u_{k1}\chi(1) \tag{54}$$

where u_{j1} and u_{k1} are constant.

Component	Parameter	Value
body	mass	3.0 kg
	length	0.40 m
	width	0.06 m
	height	0.09 m
	$c_{lb,12}$	0.12 deg^{-1}
	$c_{lb,13}$	0.03 deg^{-1}
	c_{db0}	0.0 deg^{-1}
	$c_{db,12}$	0.02 deg^{-1}
	$c_{db,13}$	0.01 deg^{-1}
	c_m	2.0 kg m^2
	A_{12}	0.04 m^2
	A_{13}	0.032 m^2
peduncle	mass	0.1 kg
	length	0.085 m
tail fin	mass	0.15 kg
	chord	0.08 m
	span	0.25 m
pectoral fins	chord	0.10 m
	span	0.35 m

TABLE I

PARAMETER VALUES FOR ROBOT CONTROL SIMULATIONS.

V. SIMULATION AND EXPERIMENTAL RESULTS

In order to evaluate the applicability and capabilities of the model developed in Sec. III, both simulations with the model and experiments with the system described in Sec. II have been performed. Parameter values used in the simulations are shown in Table I. As a note, these parameters have been chosen based on observation, not based on parameter identification, so deviation between experiment and simulation should be expected. For the experimental results, lateral and longitudinal position data comes from the vision tracking system whereas all other data (orientations and depth) was generated and processed onboard the robot. Key points to note in the results below are that the onboard orientation measurements are collected from a magnetic based device and are subject to interference from the four servos (causing noticeable noise in the data). Further, the maximum rate of the 3D compass is 8Hz and the maximum rate of the vision system is 20Hz, so experimental time constant parameters (tail joint frequencies, etc) have been chosen much slower than the upper capability of the system in order to produce data with adequate sampling.

Both open loop and closed loop control will be presented below. The first three sets of results are open loop and respectively demonstrate forward locomotion without turning using the tail, forward locomotion and turning from biasing the tail, and forward locomotion and turning using different tail joint frequencies. Prior work with the planar version of this system demonstrated that a forward gait can be constructed by applying a sine to one tail joint and a cosine to the other, both at the same frequency. Turns can be generated in one of two ways. The first is to use the tail as a rudder by biasing the forward gait motions away from the main body line. The second, predicted by the geometric structure of the system equations (32), results by applying a cosine of one frequency to the first joint and a cosine of twice that frequency to the second joint (Lemma 4.3). As shown below, these gaits can also be realized in the free-swimming robot with its caudal
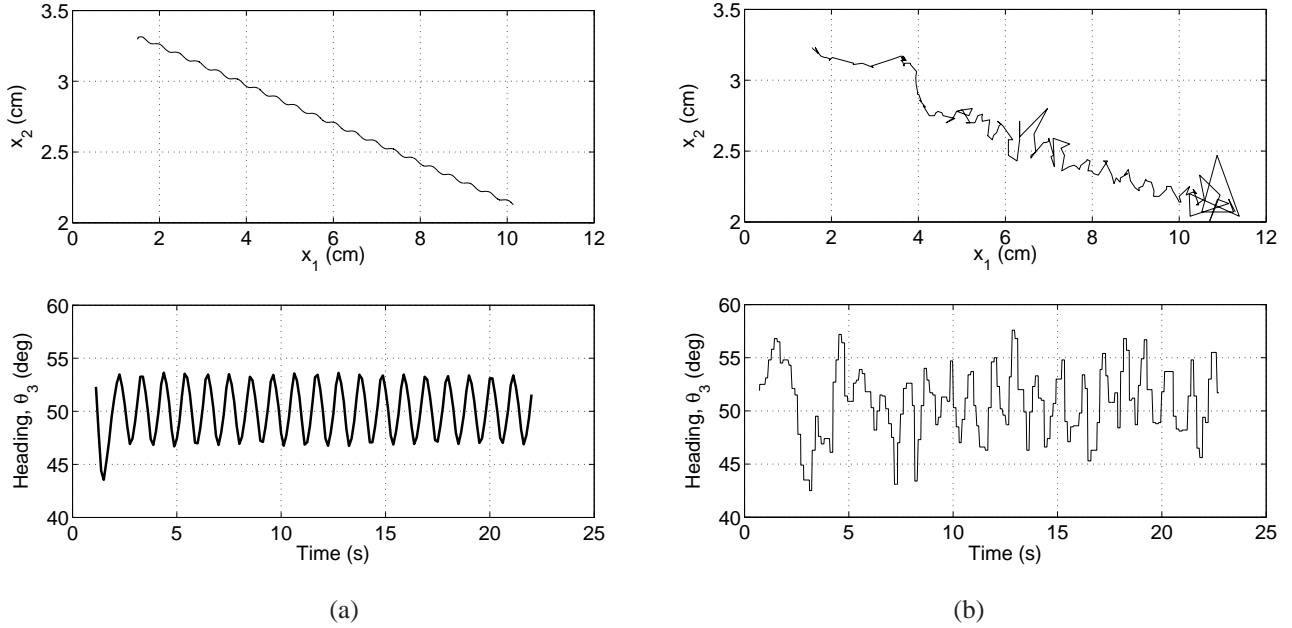
Fig. 4. Simulation (a) and experimental (b) results for open loop control of the robot to generate forward swimming using tail propulsion.

and pectoral fins.

The next three sets of results demonstrate feedback control for heading regulation with tail propulsion, depth regulation with tail propulsion, and depth regulation with pectoral fin propulsion. As has been demonstrated in earlier work with the planar system [5] and in the mathematical development [70], by evaluating the actual and desired system configurations and velocities after each oscillatory cycle, an error function can be generated and used to modify the cyclic actuation of the system. The feedback terms are only updated after whole cycles of oscillation in order to average out the naturally induced oscillation in the body from the underlying gross system motion. For the full mathematical details, we refer the reader to [70].

The final set of results is open loop and demonstrates an initial comparison of the model with experiment for agile maneuvering in the form of a snap turn. The controls for this maneuver were determined from a least squares fit of live fish data to the robot dimensions. Details are given below, but the results indicate that the model does indeed capture the key elements of agile maneuvering.

1) Open loop forward locomotion: As stated in Section IV, forward motion from oscillation of the tail can be achieved by inducing motion in the Lie bracket direction $[[f_0, f_1], [f_0, f_2]]$. Using the results above, this direction can be generated by the controls

$$u_1 = u_{11} \sin\left(\frac{2\pi}{T}\omega t\right), \ u_2 = u_{21} \cos\left(\frac{2\pi}{T}\omega t\right). \quad (55)$$

Applying these controls to both the simulation of the free-swimming robot and the experimental system gives the result shown in Fig. 4. In this case, the control parameters are $u_{11} = 30$ deg, $u_{21} = 30$ deg, $\frac{2\pi}{T}\omega = 344$ deg·s^{-1}.

Overall the general scale and magnitude of the net motion in

both translation and rotation is quite similar. The experimental system does demonstrate slightly larger body oscillations that the simulated system (most clearly seen in the region where $x_1 \in [8, 10]cm$). As mentioned above, the experimental system is subject to noise in all of the plotted variables. Given this noise, the low sampling rates of the sensors, and the modeling simplifications, the results are quite reasonable.

2) Open loop turning from biased forward locomotion: Using the above controls for open loop forward locomotion, but with a tail offset, results in a constant turn rate when the forward speed of the robot is constant. The controls that generate this motion are given by

$$u_1 = u_{11} \sin\left(\frac{2\pi}{T}\omega t\right) + \gamma, \ u_2 = u_{21} \cos\left(\frac{2\pi}{T}\omega t\right) + \gamma \quad (56)$$

with results shown in Fig. 5 for $\gamma = 10$ deg. Again, the effects of sampling rates, measurement noise and parameter mismatch are apparent. However, even given these issues, the results are qualitatively quite similar, and the scale of motion is not unreasonable. The experimental system clearly has greater translational motion, but the net heading change is almost identical to the simulation. As with the previous experiment, the results are quite reasonable.

3) Open loop turning from two frequency tail gait: The vector field $[f_1, [f_0, [f_1, [f_0, f_2]]]]$ has been indicated above to generate motion in the yaw direction of the vehicle using motion of the tail. This motion is higher order than forward locomotion and therefore results in smaller body motion magnitude than a vector field direction composed of fewer Lie brackets. As such, a biological system likely would not use it, but it is of interest from a theoretical point of view. Control functions that will generate this motion are predicted
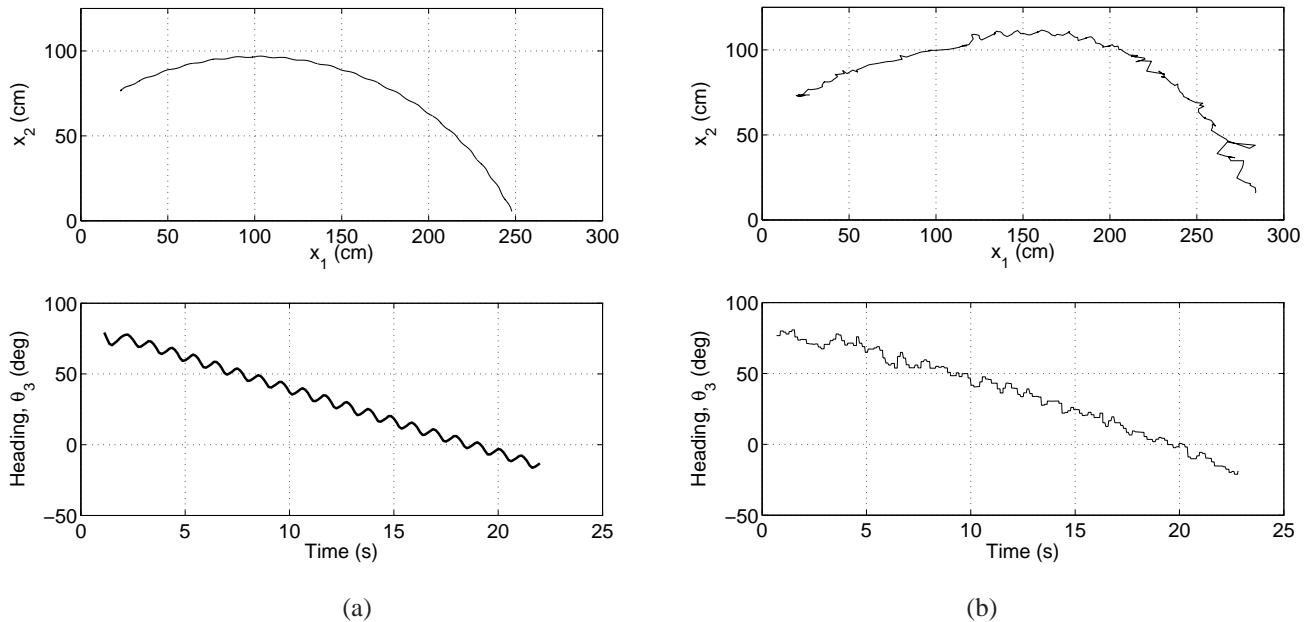
Fig. 5. Simulation (a) and experimental (b) results for open loop control of the robot to generate forward swimming with turning using biased tail propulsion.

from Lemma 4.3 to be

$$u_1 = u_{11} \cos\left(\frac{2\pi}{T}\omega t\right), \quad u_2 = u_{21} \cos\left(\frac{4\pi}{T}\omega t\right). \quad (57)$$

Using the parameters $u_{11} = 30$ deg, $u_{21} = 30$ deg, $\frac{2\pi}{T}\omega = 172$ deg·s^{-1}, simulation and experimental results for these controls are shown in Fig. 6. A clear turn occurs about the x_3 axis with a small drift (less than 10cm each direction) in the body position.

The qualitative and quantitative results of simulation are quite similar with those from experiment. The experimental system has slightly larger magnitude translation and net orientation change, but the difference is on the order of less than a centimeter in translation and 10-15 degrees in orientation. As with the other open loop maneuvers, these discrepancies would likely be minimized by performing an optimized parameter identification of the experimental system. However, for the stated goals here of exploring the connection between behavior of the model relative to behavior of the experimental system, the results are acceptable.

4) Closed loop heading control with tail propulsion:
Regulated heading control is implemented here by controlling the tail bias rather than by using the dual-frequency tail gait. The feedback structure is based on comparing measurements over whole oscillation cycles as discussed above. To track desired headings θ_{3d}, the control inputs then have the form

$$u_1 = \alpha_1 \sin(\frac{2\pi}{T}\omega t) + \gamma, \quad u_2 = \alpha_2 \cos(\frac{2\pi}{T}\omega t) + \alpha_\gamma \gamma, \ (58)$$

where $\gamma = -k_p e_\theta - k_d \dot{e}_\theta - k_i \int e_\theta$. The error terms, $e_\theta = \theta_{3d} - \theta_3$ were based on averages over whole periods of oscillation. Heading feedback data is read from the compass. Fig. 7 shows data for the use of these control functions with tail joint amplitudes $\alpha_1 = 27°$, $\alpha_2 = 30°$, $\alpha_\gamma = 1.5$,

$\frac{2\pi}{T}\omega = 1.9$Hz, $k_p = 1.0$ deg^{-1}, $k_d = 3.0$ deg^{-1}·s, and $k_i = 1.0$ (deg·s)$^{-1}$. The light dashed lines represent the target heading, which changes by $90°$ increments at certain instants. For this experiment, the robot was set to run at a fixed depth. Clearly, the experimental system required larger joint angles in order to track heading and did not respond as quickly as the simulated system for the same gains and operation parameters, however, the general tail joint behavior was qualitatively quite similar and the experimental system did meet the tracking requirements.

5) Closed loop depth control with tail propulsion: To generate pitch actuation using nonoscillatory motions for the pectoral fins and oscillatory actuation of the tail, the forward locomotion controls from the previous task were combined with feedback control of the pectoral fin angles. For this task, the pectoral fin angles were set to the same value, but they have been constructed to be capable of differential drive for other purposes. Superimposing the controls for tail thrust generation and pectoral fin lift generation, control functions become

$$u_1 = \alpha_1 \sin(\tfrac{2\pi}{T}\omega t), \quad u_2 = \alpha_2 \cos(\tfrac{2\pi}{T}\omega t), \quad (59)$$
$$u_3 = u_4 = -k_p e_x - k_d \dot{e}_x - k_i \int e_x, \quad (60)$$

where $e_x = x_{3d} - x_3$. Fig. 8 shows data for the use of these control functions with tail joint amplitudes $\alpha_1 = 27$ deg, $\alpha_2 = 30$ deg, $\frac{2\pi}{T}\omega = 1.9$ Hz, $k_p = 0.25$ deg/cm, $k_d = 0.39$ degs/cm, and $k_i = 0$ deg/cms (no integral control was used). The pectoral fin joints were limited to a maximum pitch of 34 deg, and the integral term is limited to a maximum value of 3.3 cms to prevent windup effects.

The robot was started at the surface and given a target depth of 91 cm, followed by a new target depth of 122 cm half way through the run. The pectoral fins initially set to their maximum value to produce as much motion downwards as
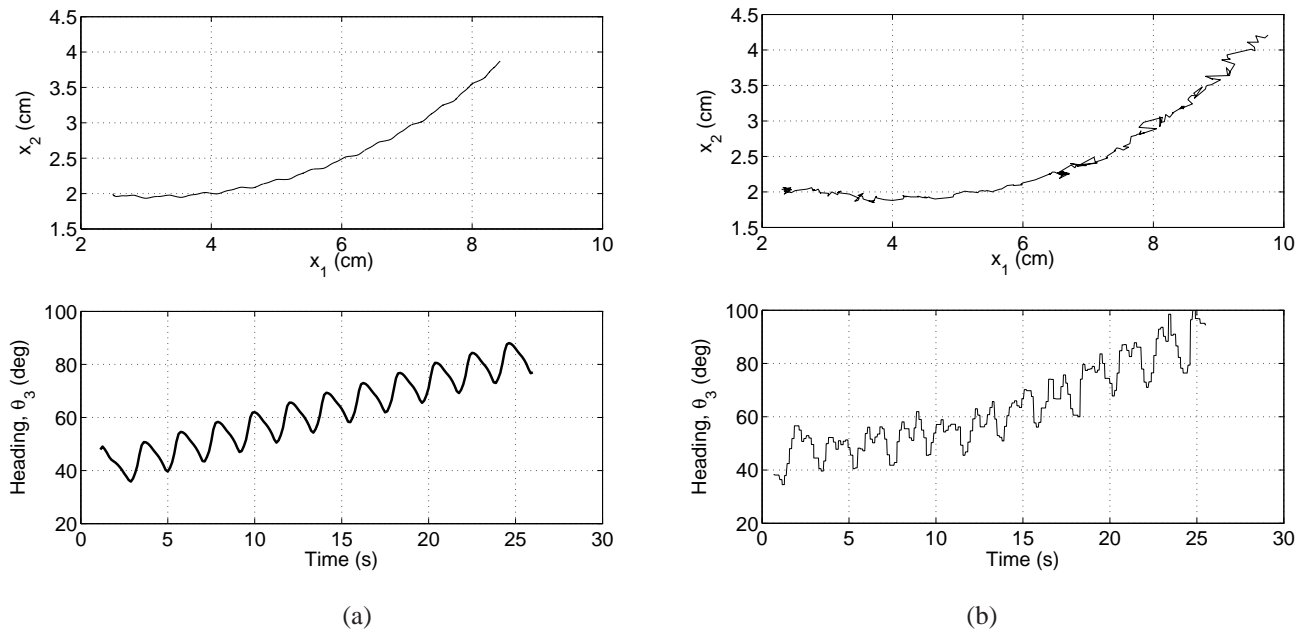
Fig. 6. Simulation (a) and experimental (b) results for open loop control of the robot to generate forward swimming with turning using different, integrally related tail joint frequencies.
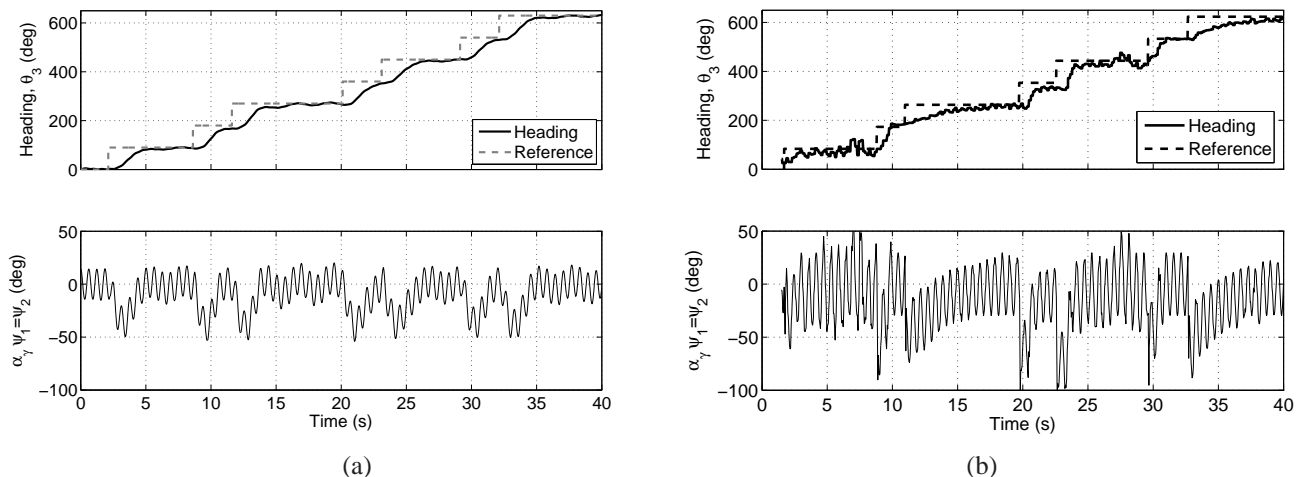

Fig. 7. Simulation (a) and experimental (b) results of closed loop heading control generated by tail joint biasing.

possible. The fin control then drove the error to within 10 cm of the desired value of 91 cm below the surface of the water, and then to the new target depth of 122 cm, where the robot then maintained the depth error within ±10 cm before the target depth was again changed to 91cm. As with the heading control, more effort was required for the experimental system to perform the desired tack than for the simulated system. Most likely this result is due to unmodeled or poorly modeled physical parameters. Note that at the beginning of the experimental run, the pectoral fins were at their pitch limit. The overall magnitude of pectoral fin pitch was of the same order for both simulation and experiment, although the settling time was not as fast in the experiment as in the simulation. Overall, however, the results are quite reasonable.

6) Closed loop depth control with pectoral fin propulsion: The final feedback results consider the effect of using the pectoral fins for both propulsion and depth regulation. Given the small size of these fins compared to the caudal fin, the motions were not as large as those generated by tail actuation. However, for the purposes of small scale maneuvering, such gaits may have importance in engineered systems. The vector fields $[f_3, [f_0, f_3]]$ and $[f_4, [f_0, f_4]]$ have equal forward motion and opposite yaw motion for identical input parameters. Applying a bias to the motion will also generate changes in depth. This effect can be used for depth control similarly to that demonstrated above for tail propulsion. To this end, the controls

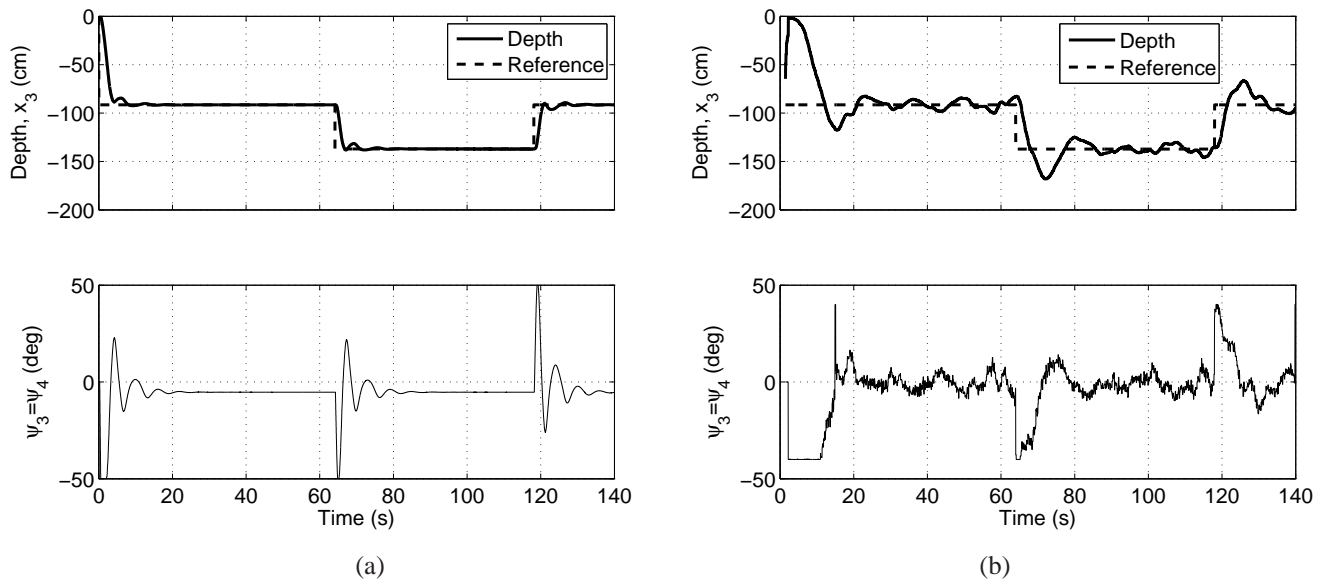$$u_3 = u_4 = \alpha_{34} \sin\left(\frac{2\pi}{T}\omega t\right) + \gamma \qquad (61)$$

Fig. 8. Simulation (a) and experimental (b) results for depth control using tailfin propulsion and pectoral fin pitch actuation.
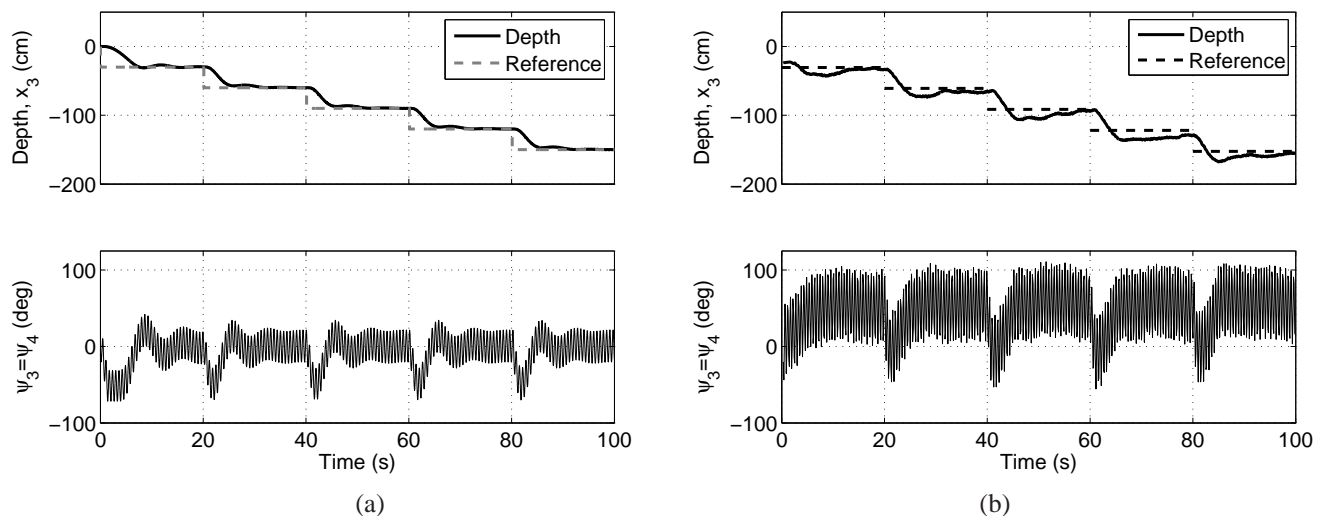

Fig. 9. Simulated (a) and experimental (b) depth regulation using pectoral fin actuation for both propulsion and depth regulation.

where $\gamma = -k_p e_x - k_d \dot{e}_x - k_i \int e_x$ and $e_x = x_3 - x_{3d}$ were used to produce the depth regulation results shown in Fig. 9. The control parameters were $\alpha_{34} = 25$deg, $\frac{2\pi}{T}\omega = 1.9$Hz, $k_p = 0.25$ deg/cm, $k_d = 0.063$ degs/cm, and $k_i = 0.25$ deg/cms. Comparing the simulation and experimental results demonstrates that, again, the experimental system had to use more effort to achieve the given tracking task and the settling time was longer. Also, in the experimental system, the steady state offset of the pectoral fins is not zero as the system is positively buoyant, requiring the fins to constantly work to maintain a fixed depth. Overall, however, the results are acceptable.

7) Agile maneuvering: As discussed in the introduction, live fish are capable of performing agile maneuvers such as fast-starts and snap-turns, which are characterized by a single non-periodic, or transient, motion. While these behaviors have not been studied as thoroughly as steady locomotion or other periodic behaviors, the use of transient effects may have connections to optimization tasks for engineered systems. As with the other fin-actuated devices used to demonstrate fast-starts and snap turns, the fin-actuated robot presented in this paper is capable of producing these maneuvers. However, no prior work has addressed the construction and evaluation of an analytic dynamics model able to replicate these behaviors. Clearly such a model has significant usefulness for purposes of control synthesis for fin-actuated vehicles and for studies of live fish behaviors. In order to evaluate the model in Sec. III for its ability to produce reasonable transient responses of fin-actuated vehicles, images of goldfish spinal shape during a snap turn behavior [14] were digitized. A least squares optimization was then used to find joint angles that produce a robot configuration that matches, as closely as possible, the
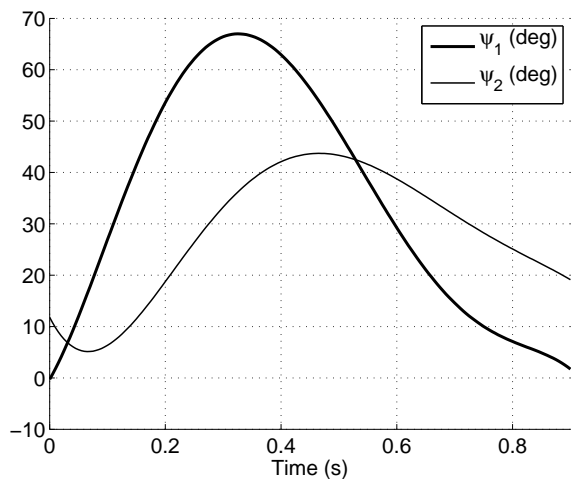
Fig. 10. Joint angle patterns for snap turn in robotic system using least squares fit of data from live fish.

goldfish shape. These values were then spline fit to create smooth joint angle functions (Fig. 10) that were used to generate the results in Fig. 11. The amplitude of the motion was scaled with a constant parameter α to produce larger angular changes. Note that for the purposes here of evaluating the model for its ability to generate transient behaviors, the particular means of finding controls that generate a snap turn in the physical system are not so important as the end result of a snap turn being produced.

The heading angle in the experimental results was captured using the on-board magnetic compass. Due to the low data rate of the compass, the data is somewhat noisy, but clearly the vehicle demonstrates a sharp, non-periodic change in orientation with the given controls. In both the experiment and the simulation, an initial sharp turn is followed by a small return, then a more slowly increasing orientation. The results in both cases are qualitatively similar, although the initial sharp turn in the simulation is much smaller than in experiment and the final slower orientation change is much larger. The difference in net motion and component magnitudes is likely due to a mismatch of lift and drag coefficients as well as added mass approximations between the model and the physical system. However, the results do indicate that the simulation will produce agile motions of the type possible in physical systems.

VI. Conclusions and future work

In the work presented here, techniques from geometric modeling and nonlinear control theory have been applied to the task of control synthesis for a fin-actuated robot. A great deal of the prior work in this area has focused on the use of kinematic models and numerical methods that do not permit the development of analytical control theoretic techniques. While the model being used is quite simplistic, the given results demonstrate that the given simplified model is sufficient as a design tool for these operation conditions. Clearly, a more accurate model, with higher order fluid effects, would lead to better response in the simulated system. Additionally,

performing a parameter fit between the experimental system and the simulation would lead to greater agreement in the results. These points are the topic of ongoing work with this system.

Given the demonstrated agreement, at least qualitatively, between the model and experiment, a number of control theoretic questions can be addressed. Of particular interest is the development of tests for controllability that are applicable to the type of system here where existing tests fail for initial conditions with zero velocity (such as when lift and drag are incorporated into dynamics models). With respect to the snap turn behavior specifically, the given results for the experimental system are reasonable, and the fact that the simulation agrees at least qualitatively indicates that the model can be used to address some questions regarding transient behaviors that are generally considered to require unsteady forces. Exactly how far this model can be taken, and how much it can be improved by the use of more accurate parameters or more accurate accounting of added mass, remains to be seen, but the implications for development of analytical methods are promising.

VII. Acknowledgements

References

[1] S. Childress, *Mechanics of Swimming and Flying*. Cambridge: Cambridge University Press, 1981.

[2] J. L. Lighthill, *Mathematical Biofluiddynamics*. Philadelphia: SIAM, 1975.

[3] J. N. Newman and T. Y. Wu, "Hydrodynamical aspects of fish swimming," in *Swimming and Flying in Nature, Vol 2.*, T. Wu, C. Brokaw, and C. Brennen, Eds. New York: Plenum, 1975, pp. 615–34.

[4] K. A. Morgansen, V. Duindam, R. J. Mason, J. W. Burdick, and R. M. Murray, "Nonlinear control methods for planar carangiform robot fish locomotion," in *Proceedings of the IEEE International Conference on Robotics and Automation*, 2001.

[5] K. Morgansen, P. Vela, and J. Burdick, "Trajectory stabilization for a planar carangiform robot fish," in *Robotics and Automation, 2002. Proceedings. ICRA '02. IEEE International Conference on*, vol. 1, 11-15 May 2002, pp. 756–762vol.1.

[6] K. A. Morgansen, "Geometric methods for modeling and control of a free-swimming carangiform fish robot," in *Proceedings of the 13th International Symposium on Unmanned Untethered Submersible Technology*, Aug. 2003.

[7] K. A. Morgansen, J. W. Burdick, J. Radford, and P. A. Vela, "Dynamics and control of a planar carangiform robot fish," in preparation.

[8] P. A. Vela, K. A. Morgansen, and J. W. Burdick, "Underwater locomotion from oscillatory shape deformations," in *Proceedings of the IEEE Conference on Decision and Control*, 2002, pp. 2074–2080.

[9] M. Sfakiotakis, D. Lane, and J. Davies, "Review of fish swimming modes for aquatic locomotion," *Oceanic Engineering, IEEE Journal of*, vol. 24, no. 2, pp. 237–252, April 1999.

[10] J. Colgate and K. Lynch, "Mechanics and control of swimming: a review," *Oceanic Engineering, IEEE Journal of*, vol. 29, no. 3, pp. 660–673, July 2004.

[11] P. Bandyopadhyay, "Trends in biorobotic autonomous undersea vehicles," *Oceanic Engineering, IEEE Journal of*, vol. 30, no. 1, pp. 109–139, Jan. 2005.

[12] S. W. Churchill, *Viscous Flows: The Practical Use of Theory*. Butterworth, 1988.

[13] M. J. Wolfgang, J. M. Anderson, M. A. Grosenbaugh, D. K. P. Yue, and M. S. Triantafyllou, "Near-body flow dynamics in swimming fish," *Journal of Experimental Biology*, vol. 202, no. 17, pp. 2303–7, 1999.
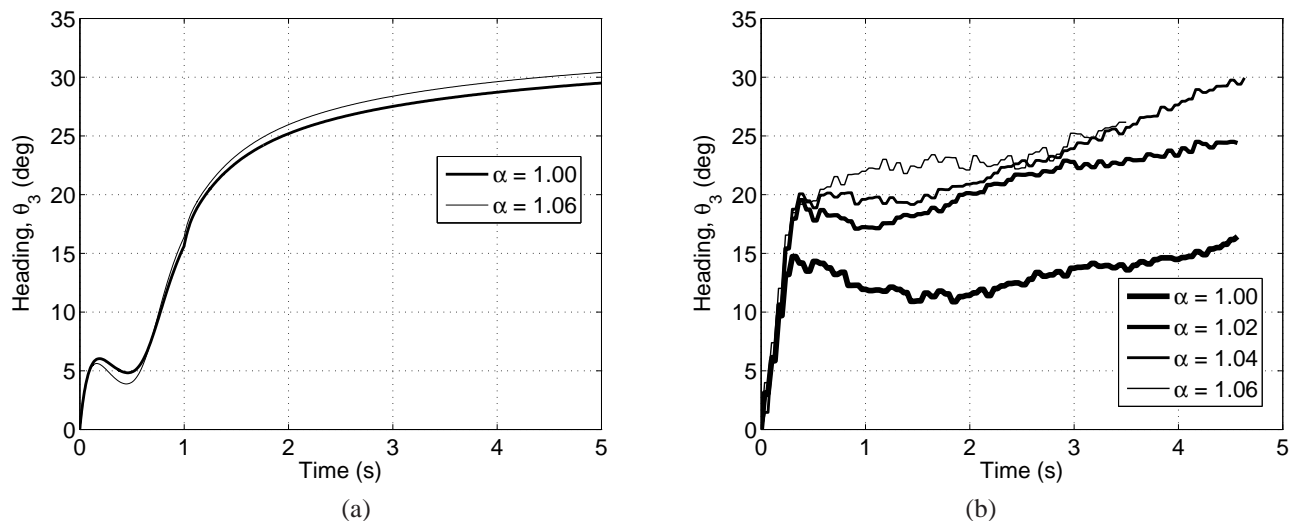
Fig. 11. Simulation (a) and experimental (b) results for snap turns.

[14] D. Weihs, "A hydrodynamical analysis of fish turning manoeuvres," *Proc. R. Soc. Lond. B*, vol. 182, pp. 59–72, 1972.

[15] ——, "The mechanism of rapid starting of slender fish," *Biorheology*, vol. 10, pp. 343–50, 1973.

[16] B. Ahlborn, D. Harper, R. Blake, D. Ahlborn, and M. Cam, "Fish without footprints," *Journal of Theoretical Biology*, vol. 148, pp. 521–33, 1991.

[17] B. Ahlborn, S. Chapman, R. Stafford, R. W. Blake, and D. Harper, "Experimental simulation of the thrust phases of fast-start swimming of fish," *Journal of Theoretical Biology*, vol. 200, pp. 2301–12, 1997.

[18] P. Domenici and R. Blake, "The kinematics and performance of fish fast-start swimming," *Journal of Experimental Biology*, vol. 200, pp. 1165–1178, 1997.

[19] S. A. Budick and D. M. O'Malley, "Locomotor repertoire of the larval zebrafish: swimming, turning and prey capture," *Journal of Experimental Biology*, vol. 203, pp. 2565–2579, 2000.

[20] I. Spiers and J. van Leeuwen, "Kinematics and muscle dynamics of C- and S-starts of carp (cyprinus carpio L.)," *Journal of Experimental Biology*, vol. 202, pp. 393–406, 1999.

[21] R. W. Blake, "Mechanics of drag-based mechanisms of propulsion in aquatic vertebrates," in *Symposium of the Zoological Society of London*, 1981.

[22] ——, *Fish Biomechanics*. Praeger Publishers, 1983, ch. Median and paired fin propulsion.

[23] E. G. Drucker and G. V. Lauder, "Locomotor forces on a swimming fish: Three-dimensional vortex wake dynamics quantified using digital particle image velocimetry," *Journal of Experimental Biology*, vol. 202, pp. 2393–2412, 1999.

[24] M. S. Gordon, J. R. Hove, P. W. Webb, and D. Weihs, "Boxfishes as unusually well-controlled autonomous underwater vehicles," *Physiological and Biochemical Zoology*, vol. 73, no. 6, pp. 663–675, Nov. 2000.

[25] J. M. Anderson, K. Streitlien, D. S. Barrett, and M. S. Triantafyllou, "Oscillating foils of high propulsive efficiency," *Journal of Fluid Mechanics*, vol. 360, pp. 41–72, 1998.

[26] J. M. Anderson and P. A. Kerrebrack, "The vorticity control unmanned undersea vehicle–an autonomous vehicle employing fish swimming propulsion and maneuvering," in *10th International Symposium on Unmanned Untethered Submersible Technology*, Durham, NH, Sept. 1997, pp. 189–95.

[27] J. M. Anderson and N. K. Chhabra, "Maneuvering and stability performance of a robotic tuna," *Integ. and Comp. Biol.*, vol. 42, pp. 118–126, 2002.

[28] D. Barrett, M. Grosenbaugh, and M. Triantafyllou, "The optimal control of a flexible hull robotic undersea vehicle propelled by an oscillating foil," in *Autonomous Underwater Vehicle Technology, 1996. AUV '96., Proceedings of the 1996 Symposium on*, 2-6 June 1996, pp. 1–9.

[29] J. Yu, M. Tan, S. Wang, and E. Chen, "Development of a biomimetic robotic fish and its control algorithm," *Systems, Man and Cybernetics, Part B, IEEE Transactions on*, vol. 34, no. 4, pp. 1798–1810, Aug. 2004.

[30] J. Yu and L. Wang, "Parameter optimization of simplified propulsive model for biomimetic robot fish," in *Robotics and Automation, 2005.*

[31] S. Licht, F. Hover, and M. Triantafyllou, "Design of a flapping foil underwater vehicle," in *Underwater Technology, 2004. UT '04. 2004 International Symposium on*, 2004, pp. 311–316.

[32] S. Wang, Z. Zhang, and H. Sang, "Analysis of velocity control algorithms for biomimetic robot fish," in *Robotics and Biomimetics, 2004. ROBIO 2004. IEEE International Conference on*, 22-26 Aug. 2004, pp. 972–976.

[33] C. Zhou, Z. Cao, S. Wang, and M. Tan, "The posture control and 3-d locomotion implementation of biomimetic robot fish," in *Intelligent Robots and Systems, 2006 IEEE/RSJ International Conference on*, Oct. 2006, pp. 5406–5411.

[34] J. Liu and H. Hu, "Simulator building and parameter optimization of an autonomous robotic fish," unpublished.

[35] J. M. Anderson, "Vortex control for efficient propulsion," Ph.D. dissertation, Join program MIT/Wood's Hole Oceanographic Institute, 1996.

[36] M. S. Triantafyllou, D. S. Barrett, D. K. P. Yue, J. M. Anderson, and M. A. Grosenbaugh, "A new paradigm of propulsion and maneuvering for marine vehicles," *Transactions of the Society of Marine Architects and Marine Engineers*, vol. 104, pp. 81–100, 1996.

[37] K. Hirata, T. Takimoto, and K. Tamura, "Study on turning performance of a fish robot," in *First International Symposium on Aqua Bio-Mechanisms*, 2000, pp. 287–292.

[38] D. Kuo and C. Eliasmith, "Understanding interactions between networks controlling distinct behaviors: Escape and swimming in larval zebrafish," *Neurocomputing*, vol. 58, 2004.

[39] J. Liu and H. Hu, "Mimicry of sharp turning behaviours in a robotic fish," in *Robotics and Automation, 2005. ICRA 2005. Proceedings of the 2005 IEEE International Conference on*, 18-22 April 2005, pp. 3318–3323.

[40] M. Ziegler, F. Iida, and R. Pfeifer, ""cheap" underwater locomotion: Morphological properties and behavioral diversity," in *International Workshop on Morphology, Control and Passive Dynamics*, 2005.

[41] J. Yu, S. Wang, and M. Tan, "A simplified propulsive model of biomimetic robot fish and its realization," *Robotica*, vol. 23, pp. 101–107, 2005.

[42] K. A. Morgansen, T. M. L. Fond, and J. X. Zhang, "Agile maneuvering for fin-actuated underwater vehicles," in *Proceedings of the International Symposium on Communication, Control and Signal Processing*, 2006.

[43] P. D. Kuo and D. Grierson, "Genetic algorithm optimization of escape and normal swimming gaits for a hydrodynamical model of carangiform locomotion," unpublished.

[44] M. M. Murray and L. E. Howle, "Spring stiffness influence on an oscillating propulsor," *Journal of Fluids and Structures*, vol. 17, pp. 915–926, 2003.

[45] K. Streitlien and M. S. Triantafyllou, "Force and moment on a joukowski profile in the presence of point vortices," *Journal of the AIAA*, vol. 33, no. 4, pp. 603–610, Apr. 1995.

[46] K. Streitlien and G. S. Triantafyllou, "On thrust estimates for flapping foils," *Journal of fluids and structures*, vol. 12, pp. 47–55, 1998.

[47] S. Kelly, R. Mason, C. Anhalt, R. Murray, and J. Burdick, "Modelling and experimental investigation of carangiform locomotion for control," in *American Control Conference, 1998. Proceedings of the 1998*, vol. 2, 24-26 June 1998, pp. 1271–1276, vol.2.

[48] S. D. Kelly and R. M. Murray, "Modelling efficient pisciform swimming for control," *International Journal of Robust and Nonlinear Control*, vol. 10, no. 4, pp. 217–41, 2000.

[49] E. Kanso, J. E. Marsden, C. W. Rowley, and J. B. Melli-Huber, "Locomotion of articulated bodies in a perfect fluid," *Journal of Nonlinear Science*, vol. 15, pp. 255–289, 2005.

[50] J. B. Melli, C. W. Rowley, and D. S. Rufat, "Motion planning for an articulated body in a perfect planar fluid," *SIAM Journal on Applied Dynamical Systems*, vol. 5, no. 4, pp. 650–669, 2006.

[51] R. J. Mason and J. W. Burdick, "Construction and modelling of a carangiform robotic fish," in *Proceedings of the International Symposium on Experimental Robotics*, 1999, pp. 235–42.

[52] R. Mason and J. Burdick, "Experiments in carangiform robotic fish locomotion," in *Robotics and Automation, 2000. Proceedings. ICRA '00. IEEE International Conference on*, vol. 1, 24-28 April 2000, pp. 428–435vol.1.

[53] J. Guo and Y.-J. Joeng, "Guidance and control of a biomimetic autonomous underwater vehicle using body-fin propulsion," *Proceedings of the Institution of Mechanical Engineers, Part M: Journal of Engineering for the Maritime Environment*, vol. 218, pp. 93–111, 2004.

[54] S. Saimek and P. Y. Li, "Motion planning and control of a swimming machine," *The International Journal of Robotics Research*, vol. 23, no. 1, pp. 27–53, 2004.

[55] E. Kim and Y. Youm, "Simulation study of fish swimming modes for aquatic robot system," in *Robotics and Automation, 2005. ICRA 2005. Proceedings of the 2005 IEEE International Conference on*, 18-22 April 2005, pp. 3330–3335.

[56] L. Wang, S. Wang, Z. Cao, M. Tan, C. Zhou, H. Sang, and Z. Shen, "Motion control of a robot fish based on cpg," in *Industrial Technology, 2005. ICIT 2005. IEEE International Conference on*, 14-17 Dec. 2005, pp. 1263–1268.

[57] G. Kosa, M. Shoham, and M. Zaaroor, "Propulsion method for swimming microrobots," *Robotics, IEEE Transactions on [see also Robotics and Automation, IEEE Transactions on]*, vol. 23, no. 1, pp. 137–150, Feb. 2007.

[58] K. McIsaac and J. Ostrowski, "Experimental verification of open-loop control for an underwater eel-like robot," *International Journal of Robotics Research*, vol. 21, no. 10-11, pp. 849–59, Oct.-Nov. 2002.

[59] ——, "Motion planning for anguilliform locomotion," *Robotics and Automation, IEEE Transactions on*, vol. 19, no. 4, pp. 637–652, Aug. 2003.

[60] F. Boyer, M. Porez, and W. Khalil, "Macro-continuous computed torque algorithm for a three-dimensional eel-like robot," *Robotics, IEEE Transactions on [see also Robotics and Automation, IEEE Transactions on]*, vol. 22, no. 4, pp. 763–775, Aug. 2006.

[61] F.-C. Chiu, C.-K. Chen, and J. Guo, "A practical method for simulating pectoral fin locomotion of a biomimetic autonomous underwater vehicle," in *Underwater Technology, 2004. UT '04. 2004 International Symposium on*, 2004, pp. 323–329.

[62] N. Kato and T. Inaba, "Hydrodynamic characteristics of apparatus of pectoral fin motion," *Journal of the Society of Naval Architects of Japan*, vol. 182, pp. 129–139, 1997.

[63] K. McIsaac and J. Ostrowski, "Motion planning for dynamic eel-like robots," in *Robotics and Automation, 2000. Proceedings. ICRA '00. IEEE International Conference on*, vol. 2, 24-28 April 2000, pp. 1695–1700vol.2.

[64] P. Valdivia y Alvarado and K. Youcef-Toumi, "Performance of machines with flexible bodies designed for biomimetic locomotion in liquid environments," in *Robotics and Automation, 2005. ICRA 2005. Proceedings of the 2005 IEEE International Conference on*, 18-22 April 2005, pp. 3324–3329.

[65] T. Wang, J. Liang, G. Shen, and G. Tan, "Stabilization based design and experimental research of a fish robot," in *Intelligent Robots and Systems, 2005. (IROS 2005). 2005 IEEE/RSJ International Conference on*, 2-6 Aug. 2005, pp. 954–959.

[66] E. Kanso and J. Marsden, "Optimal motion of an articulated body in a perfect fluid," in *Decision and Control, 2005 and 2005 European Control Conference. CDC-ECC '05. 44th IEEE Conference on*, 12-15 Dec. 2005, pp. 2511–2516.

[67] N. Kato, "Application of swimming functions of aquatic animals to autonomous underwater vehicles," in *OCEANS '99 MTS/IEEE. Riding the Crest into the 21st Century*, vol. 3, 13-16 Sept. 1999, pp. 1418–1424vol.3.

[68] ——, "Control performance in the horizontal plane of a fish robot with mechanical pectoral fins," *Oceanic Engineering, IEEE Journal of*, vol. 25, no. 1, pp. 121–129, Jan. 2000.

[69] N. Kato, Y. Ando, and T. Shigetomi, "Precision maneuvering of underwater robot by mechanical pectoral fins," in *Underwater Technology, 2004. UT '04. 2004 International Symposium on*, 2004, pp. 303–310.

[70] P. Vela, K. Morgansen, and J. Burdick, "Second order averaging methods for oscillatory control of underactuated mechanical systems," in *Proceedings of the American Control Conference*, 2002, pp. 4672–4677.

[71] M. S. Triantafyllou and G. S. Triantafyllou, "An efficient swimming machine," *Scientific American*, pp. 64–70, Mar. 1995.

[72] X. Deng and S. Avadhanula, "Biomimetic micro underwater vehicle with oscillating fin propulsion: System design and force measurement," in *Robotics and Automation, 2005. ICRA 2005. Proceedings of the 2005 IEEE International Conference on*, 18-22 April 2005, pp. 3312–3317.

[73] H. Yamaguchi and N. Bose, "Oscillating foils for marine propulsion," in *Proceedings of the Fourth (1994) International Offshore and Polar Engineering Conference*, 1994.

[74] D. A. Read, F. S. Hover, and M. S. Triantafyllou, "Forces on oscillating foils for propulsion and monitoring," *Journal of Fluids and Structures*, vol. 17, pp. 163–183, 2003.

[75] K. Hirata, "Development of experimental fish robot," in *Sixth International Symposium on Marine Engineering*, 2000.

[76] J. Davies, D. Lane, G. Robinson, D. O'Brien, M. Pickett, M. Sfakiotakis, and B. Deacon, "Subsea applications of continuum robots," in *Underwater Technology, 1998. Proceedings of the 1998 International Symposium on*, 15-17 April 1998, pp. 363–369.

[77] B. Hobson, M. Kemp, I. L. Goff, and A. Leonessa, "Oscillating fin thrusters for multi-view classification maneuvering on mcm uuvs," in *Celebrating the path... Teaming toward the future*, Sep. 2003.

[78] S. Thrun, W. Burgard, and D. Fox, *Probabilistic Robotics*. The MIT Press, 2005.

[79] R. Y. Tsai, "An efficient and accurate camera calibration technique for 3d machine vision," in *IEEE Conference on Computer Visona nd Pattern Recognition*, 1986.

[80] ——, "A versatile camera calibration technique for high-accuracy 3d machine vision metrology using off-the-shelf tv cameras and lenses," *Robotics and Automation, IEEE Journal of [legacy, pre - 1988]*, vol. 3, no. 4, pp. 323–344, Aug 1987.

[81] H. Lamb, *Hydrodynamics*, 6th ed. Dover, 1932.

[82] C. E. Brennen, "A review of added mass and fluid inertial forces," Naval civil Engineering Laboratory, Port Hueneme, CA, Tech. Rep. CR82010, Jan. 1982.

[83] A. Bloch, P. Krishnaprasad, J. Marsden, and R. Murray, "Nonholonomic mechanical systems with symmetry," *Archive for Rational Mechanics and Analysis*, vol. 126, no. 1, pp. 21–99, 1996.

[84] A. M. Bloch, *Nonholonomic Mechanics and Control*. Springer, 2003.